

Understanding Complex Metal Hydrides via Synchrotron X-ray Absorption Spectroscopy

Tabbetta Dobbins¹, Corisma Robinson^{2,*} and Shathabish NaraseGowda^{2,**}

1. Rowan University, Glassboro, NJ, U.S.A.

2. Louisiana Tech University, Ruston, LA, U.S.A.

* Currently at Grambling State University, Grambling, LA, U.S.A.

** Currently at Intel Corp., Oregon, U.S.A.

Synchrotron light sources provide high flux X-rays for performing local electronic and atomic structure studies around the constituent atoms. In this study, the local structure around TiCl_3 catalysts in the complex metal hydride NaAlH_4 reveal the gradual transformation from 3+ to 0 oxidation state and corresponding local crystal structures similar to TiAl and TiAl_3 . Nano-confinement of NaAlH_4 into the metalorganic framework, Fe-BTC, reveals that the local atomic structure around open metal site, Fe^{3+} , on the host structure retains its oxidation state but that the local atomic structure is changed by the insertion of the NaAlH_4 . A structure similar to iron acetate is found in the bare Fe-BTC and the NaAlH_4 infiltrated Fe-BTC material.

1. Introduction

Power generation in the U.S. is dominated by the use of fossil fuels. These fuels are typically burned in combustion engines to yield by-products, including CO_2 , which could contribute to environmental degradation. Of the fossil fuels used, 33% are imported natural gas and petroleum [1]. This could potentially lead to fluctuations in availability based on political landscapes. Figure 1a highlights the power generation sources for the U.S. When we consider power consumption (shown in Figure 1b), quite a large share is utilized in the transportation industry, where only light weight and mobile methods for energy production are suitable. These factors lead to the possibility for hydrogen fuel cells to penetrate the energy markets, particularly in the transportation sector. Yet, challenges remain in employing these fuel cells, including the approach for on-board, safe storage of hydrogen gas.

Complex metal hydrides are a class of materials for which hydrogen is found in the interstitial sites of the unit cell. These materials are able to store 3-12 wt. % hydrogen (at room temperature) and release it (at elevated temperatures of 100°C - 300°C) for intake into hydrogen fuel cells. Other options for hydrogen storage are (1) as a compressed gas, (2) under cryostat as liquid hydrogen, (3) as a chemical hydride (e.g. ammonia), and (4) physisorbed onto high surface area materials.[2] Of these approaches, chemical hydrides have proven the most promising for high density of hydrogen under moderate conditions. The U.S. Department of Energy has set forth targets of reduced operating temperatures (near to 80°C), fast kinetics as indicated by startup times under 15 seconds, and delivery from highly stable phases in the system as indicated by greater than 90% recoverable useable amount and high cycle life [3], [4].

Earlier work reveals that the hydrogen gas desorption temperature might be tuned by (i) catalysts

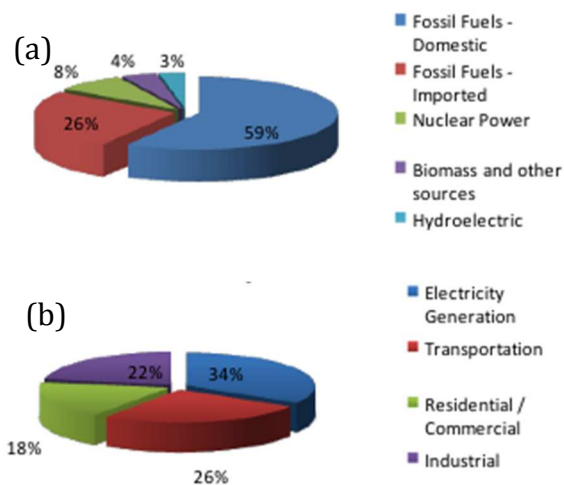
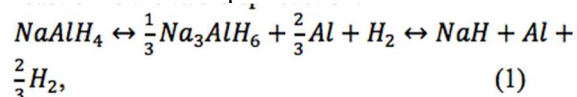


Figure 1. (a) Power Generation and (b) Power Consumption modalities for the U.S. Data is from Reference [1].

[5]–[8] and (ii) nano-structuring [9]–[14]. Many studies have been performed on the complex metal hydride, sodium alanate, NaAlH_4 . It is also known as sodium aluminum hydride (SAH). This compound first proven reversible in work done by Bogdanovic and Schwickardi [5] after catalyzing with titanium. The reversible reaction is the two-step reaction:



Subsequently, Anton showed that titanium catalysts (among many other transition metal catalysts) improved the desorption kinetics [6]. Together, these studies led to a dichotomy in understanding the role of the titanium catalysts. On the one hand, these catalysts improve the desorption reaction [6] and on the other, the same catalyst makes possible the reverse reaction [5]. Furthermore, Sandrock et al. [7] showed that the reversible hydrogen storage capacity is decreased with

increasing amounts of titanium catalysts. Potentially, the titanium acts as a dopant, mitigating diffusion rates for enhanced desorption, in addition to playing the role of a catalyst for the hydrogen uptake reaction. Synchrotron X-ray Ultrasmall Angle X-ray Scattering (USAXS) showed that, relative to other dopants, TiCl_3 doped NaAlH_4 particles have a higher surface area after five minutes of high energy ball milling [8]. Other approaches to lower the hydrogen desorption temperature from sodium alanate is to nanostructure the hydride [9]–[12], [15], [16]. This is accomplished by vacuum infiltration into metallographic framework (MOF) structures having pore sizes in the 3–5 nm range [9], [10]. Studies performed on nanostructured hydrides, within MOFs, revealed that both hydrogen dynamics and reaction mechanisms for desorption are changed [9].

Hence, studies which are able to reveal the local structure of the titanium species (which is added in 2mol% to 4mol% quantities) such as X-ray absorption spectroscopy using synchrotron light sources are deemed useful. Likewise, for NaAlH_4 nano-confined within MOFs, whether the metal sites on the MOF are active in binding with the NaAlH_4 lattice could also be elucidated by local structure studies. In already published work, such studies were employed on Ti-catalyzed complex metal hydrides [8], [14], [17]–[19] to reveal that amorphous TiAl_3 is formed during dehydrogenation cycling [19]. Fichtner et al. showed that nm-Ti metal is found in the ball milled NaAlH_4 [18].

This manuscript presents results of synchrotron X-ray absorption spectroscopy (XAS) studies performed on two material systems (i) TiCl_3 catalysts added to NaAlH_4 and (ii) NaAlH_4 nano-confined in the MOF Fe-BTC. This paper is intended to shed light on (1) the pathway to formation of TiAl_3 observed in prior studies and (2) to local structure of metal site (Fe^{x+}) on the MOF after insertion of NaAlH_4 .

2. Experimental Methods

Samples were prepared by ball milling NaAlH_4 for 30 minutes using a Spex 8000 mill, a steel vial, and steel milling media. The milled NaAlH_4 was then blended with 2 mol % TiCl_3 . Some blended material was reserved for analysis; the rest was separated into different samples that were milled for 1 minute, 5 minutes, 25 minutes, or 125 minutes. The milled TiCl_3 -doped NaAlH_4 was then separated again; some material was reserved for analysis while other material was processed through a hydrogen desorption-absorption cycle in a pressure-composition-isotherm (PCI) apparatus from Advanced Materials Corporation (Pittsburgh, PA). The TiCl_3 -doped NaAlH_4 was dehydrogenated at 150°C in 0.4 atm H_2 and were recharged at 150°C at 160 atm H_2 .

NaAlH_4 was confined within the porous structure of commercial Fe-benzenetricarboxylate (Fe-BTC) by solution infiltration using tetrahydrofuran (THF) as the precursor solvent. Sodium aluminum hydride, NaAlH_4 , THF and Fe-BTC were used as purchased (Sigma Aldrich). First, NaAlH_4 was ball-milled for 5 min in a high-energy planetary ball-mill (8000M CertiPrep Spex Metuchen, NJ) to remove aggregates. The powdered NaAlH_4 sample was mixed thoroughly in THF to make a precursor solution with a concentration of $\approx 10\text{mg/ml}$. Fe-BTC was heated to a temperature of 200°C for four hours to remove any adsorbed moisture and volatiles. The NaAlH_4 -THF precursor was mixed with Fe-BTC in a 1:1 ratio by weight and subsequently vacuum dried for 8–10 min. The use of vacuum, in addition to removing THF, helps to drive the NaAlH_4 particles into the pores of the Fe-BTC.

Samples were sealed within KaptonTM tape within a dry N_2 glovebox and were subsequently loaded into a N_2 filled sample chamber at the Double Crystal Monochromator (DCM) beamline, Center for Advanced Microstructures and Devices (CAMD), Baton Rouge, LA. CAMD operates an electron storage ring at 1.3 GeV. The key components of the X-ray absorption spectroscopy (XAS) beamline at CAMD are found in reference [8]. Germanium (220) mono-chromator crystals with 0.1 eV step sizes were used for tuning x-ray energy in the vicinity of the absorption Fe and Ti K-shell absorption edges. The beamline was calibrated at the Ti and Fe K edges with the respective metal foils. The Ti K-shell was calibrated to 4966 eV and the Fe K-shell was calibrated to 7112eV [20]. XAS data were collected in fluorescence mode. Step sizes used were 2.0 eV for the first 60 eV of pre-edge data, 0.3 eV for the following 40 eV XANES spectra, and 1.0 eV for the remaining 1000 eV EXAFS spectra. A 13 element CanberraTM detector (Meriden, CT) was used to collect the fluorescence signal. Two spectra were collected from each sample and the average is reported. WINXAS software was used for EXAFS ($\chi(k)$) data extraction and Fourier transforming the EXAFS signal. A wave-vector (k^3) weighting factor was applied to the EXAFS data in order to emphasize the analysis of high k (low distance) region. For NaAlH_4 nano-confined within MOFs, the Iffeffit software package was used [21].

3. Theoretical Aspects to Analysis of X-ray Absorption Spectroscopy (XAS)

X-ray absorption spectroscopy (XAS) is an umbrella term which encompasses two distinct measurement techniques, X-ray absorption Near Edge Structure (XANES) which provides information about the oxidation state of the absorber atom [22] and Extended X-ray Absorption Fine Structure (EXAFS) which provide additional information about the local atomic

environment of the absorber atom [23]. Oscillations in absorption after the absorption edge, i.e. the EXAFS signal, had been observed since the 1930's and explained using the Kronig-Penney model [24]. In 1971, the currently used model for analysis of the EXAFS signal was developed by Sayers, Stern, and Lytle [25]. The EXAFS signal appears as oscillations occurring after the absorption edge—the origins of which are the modulation in absorption due to backscatter of the photo emitted electron by neighboring atoms. This backscatter phenomenon occurs to a distance of 8\AA from the absorber atom, depending on the atomic number of the absorber and neighboring atoms. Since the signal arises because of the photoemission of an electron, the local structure of the “absorber atom” is contained within the data, making the technique ideal for examination of the local structure for (1) small quantities of the absorber atom and (2) disordered systems—for which the absorber atom displays no long range order.

Synchrotron light sources, which provide tunable X-rays of high flux are capable of resolving the “weak” EXAFS oscillations. Absorption coefficient, μ , is defined within the Beer-Lambert Law

$$I = I_0 e^{-\mu t} \tag{2}$$

(where t is sample thickness, I is the measured intensity and I_0 is incident intensity). Intensity (I) data are collected as a function of energy and these data are subsequently transformed into $\mu(E)$ data. Typically, 10 eV before the absorption edge and 100eV to 1000 eV behind the absorption edge is suitable for providing the full signal. The absorption as a function of X-ray energy data, $\mu(E)$, is transformed into EXAFS data, $\chi(k)$, by the equations

$$\chi(E) = \frac{\mu(E) - \mu_0(E)}{\Delta\mu} \tag{3}$$

$$\chi(k) = \sum_j \frac{N_j f_j(k) \exp(-2k^2 \sigma_j^2)}{k R_j^2} \sin[2kR_j + \delta_j(k)] \tag{4}$$

where k is the photoelectron wave vector given by

$$k = \frac{\sqrt{2m(E - E_0)}}{\hbar} \text{ (units of } \text{\AA}^{-1}\text{),} \tag{5}$$

μ_0 is absorption for an isolated atom, $\Delta\mu$ is magnitude of the change of absorption occurring at the absorption edge, $\delta_j(k)$ is the phase shift function, f_j is the atomic form factor, N_j is the coordination for neighboring atoms, R_j atomic distances from the central absorber atom to neighboring atoms, and σ_j is the Debye-Waller disorder factor.

The Fourier Transform of the $\chi(k)$ signal provides the radial distribution function (RDF) around the absorber

atom. Since data reported here are without phase correction, it is termed pseudo-RDF data.

4. Results of X-ray Absorption Near Edge Structure (XANES) at Ti-K-edge for TiCl_3 catalyzed NaAlH_4

Figure 2 shows X-ray absorption near edge structure (XANES) data at the Ti K-edge for 2 mol.% TiCl_3 in NaAlH_4 samples milled for various times (0, 1, 5, 25, and 125 minutes). The 5, 25, and 125 minutes data show a clear shift to lower energy (4966 eV) corresponding to the transformation of Ti^{3+} to Ti^0 (absorption is found at 4969 eV) during this time period in the mixer/mill. These absorption energies were verified by measurement of standards TiN (representing Ti^{3+}) and TiAl_3 (representing Ti^0).

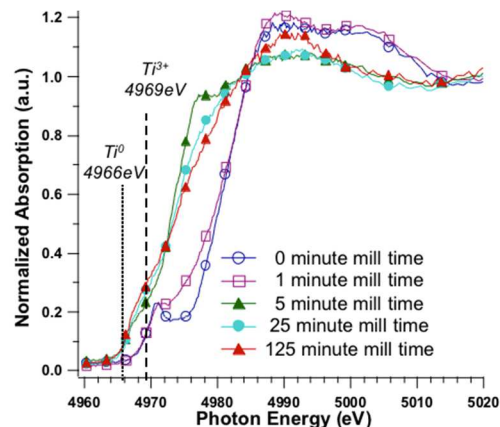


Figure 2. XANES data at the Ti K-edge of 2 mol% TiCl_3 in NaAlH_4 samples milled for 0, 1, 5, 25, and 125 minutes.

5. Results of Extended X-ray Absorption Fine Structure (EXAFS) at Ti-K-edge for TiCl_3 catalyzed NaAlH_4

This study explores chemical transitions of the 2 mol % TiCl_3 to NaAlH_4 powders during high energy ball milling using extended x-ray absorption fine structure (EXAFS) spectra. Figures 3 and 4 show the normalized absorption, $\mu(E)$, data and the corresponding RDF curves, respectively. The occurrence of two transformations are revealed. The first transformation takes place during the first 5 minutes of ball milling whereby the dopant shifts from Ti^{3+} (in TiCl_3) to a transitional state Ti^0 (in TiAl). The second transformation occurs after an additional 20 minutes of high energy milling from Ti^0 (in TiAl) to Ti^0 (in TiAl_3). The first Ti^0 state which appears is a disordered TiAl phase with bond lengths shorter than the crystalline TiAl phase. This phase exists for mill times up to 25 minutes. After 25 minutes of high energy milling, the stable TiAl_3 remains. This study reports, for the first time, the appearance of a TiAl phase as an intermediate between TiCl_3 (in the earliest 0 and 1 minutes mill times)

and $TiAl_3$ (in the latter 25 and 125 minute mill times). The RDF data collected from the sample milled for 5 minutes resemble the $TiAl$ standard. After a single desorption/absorption cycle (shown in Figures 5 and 6), the RDF around Ti appears similar to that of $TiAl_3$ for all milled samples. Those samples milled for 1 minute and 5 minutes had not shown RDF similar to $TiAl_3$ before cycling. The samples milled for 25 minutes had shown a RDF similar to $TiAl_3$ as a result of the milling operation—and it can be concluded that these $TiAl_3$ phases formed during milling were stable and remained even after the desorption cycling. These titanium containing phases are formed in quantities which are

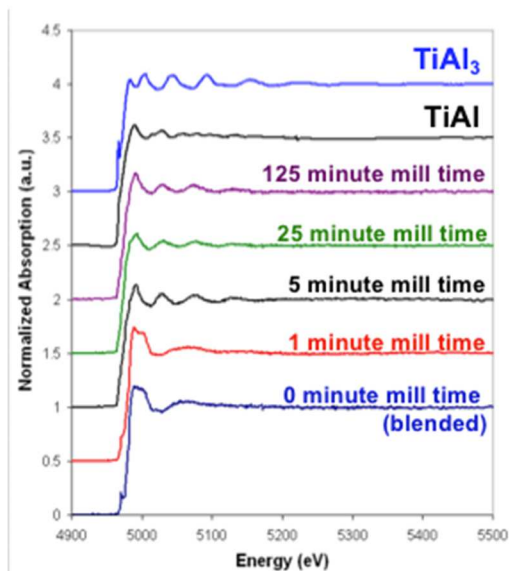


Figure 3. Absorption curves for $NaAlH_4$ with 2 mol.% $TiCl_3$ added by ball milling for 0, 1, 5, 25, and 125 minutes. Absorption curves for the $TiAl$ and $TiAl_3$ standards are included for comparison.

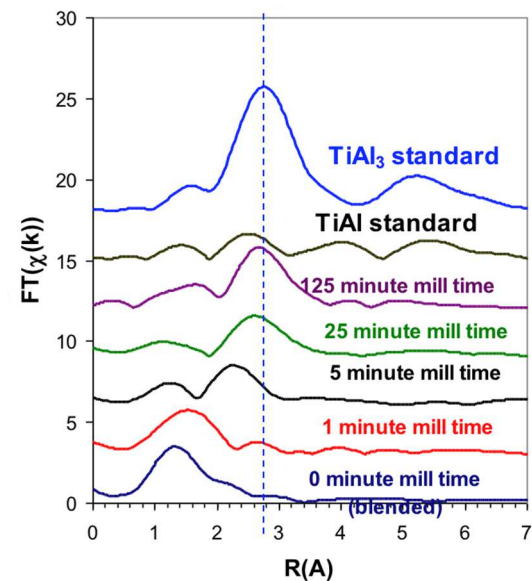


Figure 4. Pseudo-Radial Distribution Function (pseudo-RDF) curves for $NaAlH_4$ with 2 mol.% $TiCl_3$ added by

ball milling for 0, 1, 5, 25, and 125 minutes. Absorption curves for the $TiAl$ and $TiAl_3$ standards are included for comparison.

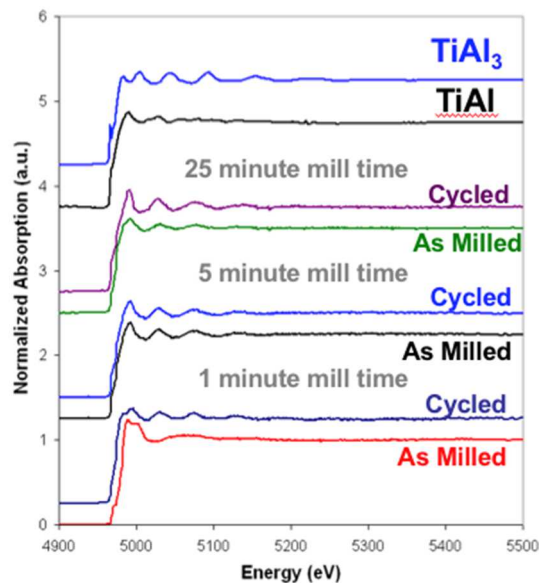


Figure 5. Absorption curves for $NaAlH_4$ with 2 mol.% $TiCl_3$ added by ball milling for 0, 1, 5, and 25 minutes. The absorption curves after a single desorption cycle are included. Absorption curves for the $TiAl$ and $TiAl_3$ standards are also included for comparison.

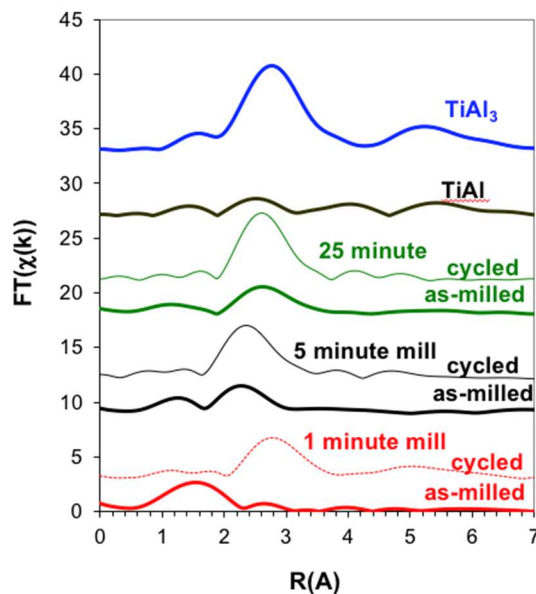


Figure 6. Pseudo-Radial Distribution Function (Pseudo-RDF) curves for $NaAlH_4$ with 2 mol.% $TiCl_3$ added by ball milling for 0, 1, 5, and 25 minutes. The absorption curves after a single desorption cycle are included. Absorption curves for the $TiAl$ and $TiAl_3$ standards are also included for comparison.

below the detection limits for x-ray diffraction. Further studies published elsewhere performed using

synchrotron X-ray photoemission electron microscopy shows that the Ti^{3+} is involved in interacting with Al^{3+} on the $NaAlH_4$ sites for form the product $TiAl$ and $TiAl_3$ phases [26].

6. Results of X-ray Absorption Spectroscopy at the Fe-K-edge for $NaAlH_4$ Nano-confined within Fe-BTC

MOFs offer a very unique pore morphology that contains unsaturated metal sites. These sites are primary interaction zones for guest molecules, making them suitable for a variety of applications [27]–[29]. X-ray absorption spectroscopy have proven to be useful in characterizing the structure of MOFs [28], [29]. The XANES spectrum of Fe-BTC best matched iron(III) acetate and thus Fe sites are believed to be in a +3 oxidation state. Dhakshinamoorthy, et al. [27] reports the same oxidation state based on their studies. The near edge features of the Basolite F before and after infiltration were identical indicating that there were no changes in the oxidation state of the Fe sites remained in a +3 state. The edge positions of Fe-BTC before and after infiltration is unchanged at 7125.4 eV. In comparison, the edge of Fe in Fe-foil was 7112 eV.

Figure 7 shows the X-ray absorption spectra for Fe-BTC and $NaAlH_4$ infiltrated Fe-BTC along with several standards (including iron acetate, iron oxide, and iron foil). The XANES data in Figure 7 reveals a largely undisturbed Fe^{3+} site after infiltration of $NaAlH_4$ into the MOF. In both cases, MOF and $NaAlH_4$ -infiltrated MOF, Fe (III) acetate provides the nearest match to the local structure around the absorber (Fe) atoms. Figure 8 shows the Fourier transformed EXAFS data in R-space (i.e. pseudo-RDF data). Since the data is not corrected for phase shift, δ_j , all distances are nominal (and could be as great as 0.5Å from the actual distance to neighboring atom). Trends in the data, not actual bond lengths, are to be assumed for the following discussion. There is a difference in the pseudo-RDF of the Basolite F (Fe-BTC) MOF before and after $NaAlH_4$ infiltration. The most evident difference is that the first peak is distorted into a superposition of two peaks in the $NaAlH_4$ -infiltrated sample. As well, the position of the peak was lowered slightly after the $NaAlH_4$ -infiltration from $\sim 1.5\text{\AA}$ in the pure Basolite F to 1.25\AA . The additional peak at $\sim 1\text{\AA}$ (in the $NaAlH_4$ infiltrated MOF) is presumed from noise since physically all bond lengths are greater than this. There is effectively no discernable difference in bond length after infiltration—since phase shift correction was not employed. There do not appear to be any additional peaks besides the one major peak in the pseudo-RDF curves indicating that there is no long range order around the Fe site.

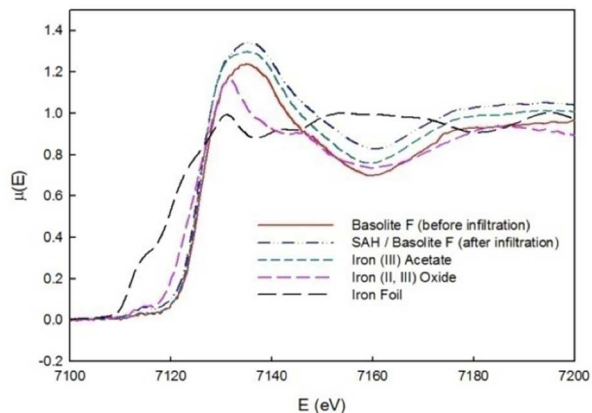


Figure 7. XANES spectra of Basolite F (Fe-BTC) before and after sodium aluminum hydride (SAH) infiltration; spectra of several Fe standards are included for comparison.

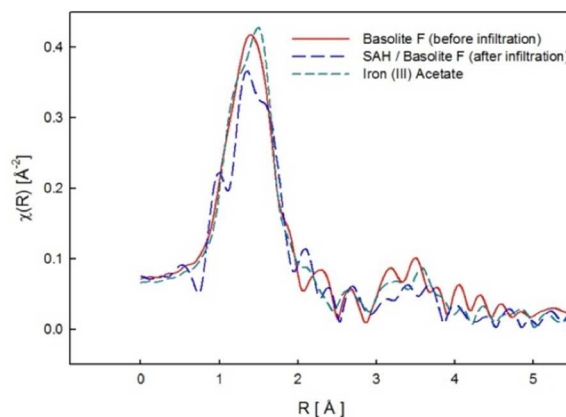


Figure 8. Pseudo-RDF Fourier transformed EXAFS spectra in R-space of Basolite F before and after sodium aluminum hydride (SAH) infiltration; Fe (III) Acetate is included for comparison.

7. Conclusions

The work presented herein has provided evidence of novel results that (1) during high energy ball milling, a $TiAl$ phase precedes the formation of $TiAl_3$ phases and (2) that during nano-confinement within MOFs, there is alteration of the metal sites on the host. These changes in the local structure around the host site are possibly due to molecular bond formation with organic solvents used as carriers for the hydride. Nano-confinement methods which does not involve the use of organic carriers should be explored by researchers wishing to understand the interaction of the host lattice with the hydride. Work which examines whether the titanium catalyst could be bound to a host structure, for example, deposited onto the nano-confinement template prior to hydride infiltration, could possibly catalyze the reaction while avoiding formation of $TiAl_3$.

For inclusion of hydrogen fuel cells in mobile power supply applications, many challenges in the safe and practical storage of hydrogen must be addressed. The present work shows that the beneficial strategies of catalytic doping with transition metals, e.g. titanium, and nano-structuring would benefit from further research. Questions remain surrounding whether the whether the intermediate phase, TiAl, could be stabilized—rather than ultimately forming TiAl₃ so as to leave more Al³⁺ sites in the NaAlH₄ for hydrogen re-adsorption to the AlH₄⁻ sub-unit. Likewise, whether the reaction to form TiAl and TiAl₃ is consequential to enhancing hydrogen gas desorption rates, uptake rates, or both is still an open question. Although nano-structuring is now well accepted as a means to alter the thermodynamics (and perhaps kinetics) of the hydrogen desorption reaction, the use of organic solvents, which could adsorb onto the host structures, must be carefully studied (along with studying the nano-structuring effects). Finally, the need for synchrotron X-ray facilities to drive new discoveries in materials for energy applications is a critical need for the continent of Africa. At the time of writing this paper, there exists no synchrotron light source on the continent. The absence of such a facility should not be a “blind spot” in the landscape for scientific infrastructure development. Fortunately, at this stage many researchers are taking advantage of several resources which provide travel support and mail-in sample measuring.

8. Acknowledgements

General support came from the NSF (Grant No. DMR1231153). Our use of the Center for Advanced Microstructures and Devices at synchrotron X-ray facility was supported by Louisiana State University, Baton Rouge, LA, U.S.A. Data were collected at the DCM beamline with the help of Mr. Gregory Merchan and Dr. Amitava Roy. Partial financial support for presentation of this work at the first biennial African Conference on Fundamental Physics and Applications (ACP2018) came from the Rowan University Research Experience for Diversity and Inclusion (REDI) program. To learn more about synchrotron light sources and funding opportunities to visit, see [30]–[32]. Follow synchrotron related updates on twitter @AfSynchrotron.

References

- [1] J. Stringer and L. Horton, “Basic Research Needs To Assure A Secure Energy Future,” *Rep. from Basic Energy Sci. Advis. Comm.*, p. 9, 2003.
- [2] S. Satyapal, J. Petrovic, and G. Thomas, “Gassing Up with Hydrogen,” *Sci. Am.*, vol. 4, pp. 81–87, 2007.
- [3] DOE Office of Science, “Basic Research Needs for the Hydrogen Economy.” [Online]. Available: https://science.energy.gov/~media/bes/pdf/reports/files/Basic_Research_Needs_for_the_Hydrogen_Economy_rpt.pdf.
- [4] A. O. Backus, *Hydrogen Energy: Background, Significance And Future*. Nova Novinka, 2006.
- [5] B. Bogdanović and M. Schwickardi, “Ti-doped alkali metal aluminium hydrides as potential novel reversible hydrogen storage materials,” *J. Alloys Compd.*, vol. 253–254, pp. 1–9, 1997.
- [6] D. Anton, “Hydrogen desorption kinetics in transition metal modified NaAlH₄,” *J. Alloys Compd.*, vol. 357, pp. 400–404, 2003.
- [7] G. Sandrock, K. Gross, and G. Thomas, “Effect of Ti-catalyst content on the reversible hydrogen storage properties of the sodium alanates,” *J. Alloys Compd.*, vol. 339, no. 1–2, pp. 299–308, 2002.
- [8] E. Bruster, T. A. Dobbins, R. Tittsworth, and D. Anton, “Decomposition behavior of Ti-doped NaAlH₄ studied using X-ray absorption spectroscopy at the titanium K-edge,” in *Materials Research Society Symposium Proceedings*, 2005, vol. 837.
- [9] S. Narase Gowda, C. M. Brown, M. Tyagi, T. A. Jenkins, and T. A. Dobbins, “Quasi-Elastic Neutron Scattering (QENS) Studies of Hydrogen Dynamics for Nano-Confined NaAlH₄,” *J. Phys. Chem. C*, p. acs.jpcc.6b02431, 2016.
- [10] P. Ngene, P. Adelhelm, A. M. Beale, K. P. De Jong, and P. E. De Jongh, “LiBH₄ / SBA-15 Nanocomposites Prepared by Melt Infiltration under Hydrogen Pressure : Synthesis and Hydrogen Sorption Properties,” *J. Phys. Chem. C*, vol. 114, no. 13, pp. 6163–6168, 2010.
- [11] J. Gao, P. Adelhelm, M. H. W. Verkuijlen, C. Rongeat, M. Herrich, P. J. M. Van Bentum, O. Gutfleisch, A. P. M. Kentgens, K. P. De Jong, and P. E. De Jongh, “Confinement of NaAlH₄ in Nanoporous Carbon : Impact on H₂ Release , Reversibility , and Thermodynamics,” *J. Phys. Chem. C*, vol. 114, no. 10, pp. 4675–4682, 2010.
- [12] S. Zheng, F. Fang, G. Zhou, G. Chen, L. Ouyang, M. Zhu, and D. Sun, “Hydrogen Storage Properties of Space-Confined NaAlH₄ Nanoparticles in Ordered Mesoporous Silica,” *Chem. Mater.*, vol. 20, no. 12, pp. 3954–3958, Jun. 2008.
- [13] R. K. Bhakta, J. L. Herberg, B. Jacobs, A. Highley, R. Behrens, N. W. Ockwig, J. a Greathouse, and M. D. Allendorf, “Metal-organic frameworks as templates for nanoscale NaAlH₄,” *J. Am. Chem. Soc.*, vol. 131, no. 37, pp. 13198–13199, 2009.

- [14] A. Léon, O. Kircher, M. Fichtner, J. Rothe, and D. Schild, "Evolution of the local structure around Ti atoms in NaAlH₄ doped with TiCl₃ or Ti13.6THF by ball milling using X-ray absorption and X-ray photoelectron spectroscopy.," *J. Phys. Chem. B*, vol. 110, no. 3, pp. 1192–200, 2006.
- [15] S. NaraseGowda, S. A. Gold, J. Ilavsky, and T. A. Dobbins, "Ultrasmall Angle X-Ray Scattering (USAXS) Studies of Morphological Changes in NaAlH₄," in *Materials Challenges in Alternative and Renewable Energy*, Hoboken, NJ, USA: John Wiley & Sons, Inc., 2011, pp. 51–59.
- [16] R. K. Bhakta, J. L. Herberg, B. Jacobs, A. Highley, R. Behrens, N. W. Ockwig, J. A. Greathouse, and M. D. Allendorf, "Metal–Organic Frameworks As Templates for Nanoscale NaAlH₄," *J. Am. Chem. Soc.*, vol. 131, no. 37, pp. 13198–13199, Sep. 2009.
- [17] A. Léon, J. Rothe, D. Schild, and M. Fichtner, "Comparative study of NaAlH₄ doped with TiCl₃ or Ti 13 · 6THF by ball milling using XAS and XPS," vol. 8, no. 1, pp. 2–7, 2005.
- [18] M. Fichtner, O. Fuhr, O. Kircher, and J. Rothe, "Small Ti clusters for catalysis of hydrogen exchange in NaAlH₄," *Nanotechnology*, vol. 14, no. 7, pp. 778–785, 2003.
- [19] J. Graetz, J. J. Reilly, J. Johnson, A. Y. Ignatov, and T. A. Tyson, "X-ray absorption study of Ti-activated sodium aluminum hydride," *Appl. Phys. Lett.*, vol. 85, no. 3, pp. 500–502, 2004.
- [20] A. Thompson, D. Attwood, G. Eric, H. Malcolm, K.-J. Kim, J. Kirz, J. Kortright, I. Lindau, P. Pianetta, A. Robinson, J. Scofield, J. Underwood, D. Vaughan, G. Williams, and H. Winick, "Center for X-ray Optics and Advanced Light Source: X-ray Data Booklet," 2001. [Online]. Available: <http://xdb.lbl.gov/>. [Accessed: 16-Jun-2018].
- [21] B. Ravel and M. Newville, "ATHENA, ARTEMIS, HEPHAESTUS: Data analysis for X-ray absorption spectroscopy using IFEFFIT," *J. Synchrotron Radiat.*, vol. 12, no. 4, pp. 537–541, 2005.
- [22] J. Stohr, *NEXAFS Spectroscopy*. Springer-Verlag Berlin Heidelberg, 1992.
- [23] B. K. Teo, *EXAFS: Basic Principles and Data Analysis*. Springer-Verlag Berlin Heidelberg, 1986.
- [24] R. de L. Kronig and W. G. Penney, "Quantum Mechanics of Electrons in Crystal Lattices," *Proc. R. Soc. A Math. Phys. Eng. Sci.*, vol. 130, no. 814, pp. 499–513, 1931.
- [25] D. E. Sayers, E. A. Stern, and F. W. Lytle, "New Technique for Investigating Noncrystalline Structures: Fourier Analysis of the Extended X-ray-Absorption Fine Structure," *Phys. Rev. Lett.*, vol. 27, no. 18, pp. 1204–1207, 1971.
- [26] T. Dobbins, M. Abrecht, Y. Uprety, and K. Moore, "An x-ray photoemission electron microscopy study of the formation of Ti-Al phases in 4 mol% TiCl₃ catalyzed NaAlH₄ during high energy ball milling.," *Nanotechnology*, vol. 20, no. 20, p. 204014, 2009.
- [27] A. Dhakshinamoorthy, M. Alvaro, and H. Garcia, "Metal organic frameworks as efficient heterogeneous catalysts for the oxidation of benzylic compounds with t-butylhydroperoxide," *J. Catal.*, vol. 267, no. 1, pp. 1–4, 2009.
- [28] C. Prestipino, L. Regli, J. G. Vitillo, F. Bonino, A. Damin, C. Lamberti, A. Zecchina, P. L. Solari, K. O. Kongshaug, and S. Bordiga, "Local Structure of Framework Cu(II) in HKUST-1 Metallorganic Framework: Spectroscopic Characterization upon Activation and Interaction with Adsorbates," *Chem. Mater.*, vol. 18, no. 5, pp. 1337–1346, Mar. 2006.
- [29] S. Bordiga, F. Bonino, K. P. Lillerud, and C. Lamberti, "X-ray absorption spectroscopies: useful tools to understand metallorganic frameworks structure and reactivity," *Chem. Soc. Rev.*, vol. 39, no. 12, pp. 4885–4927, 2010.
- [30] S. Mtingwa, "Light Sources for Africa, the Americas, Asia, and Middle East Project." [Online]. Available: <https://laamp.iucr.org/>. [Accessed: 16-Jun-2018].
- [31] "The African Light Source Conference and Workshop Booklet," 2015. [Online]. Available: www.africanlightsource.org. [Accessed: 16-Jun-2018].
- [32] S. Connell, "The African Light Source Project. Presentation slides delivered at the World Science Forum (WSF)," 2017.

Received: 11 October, 2018

Accepted: 20 October, 2018